ELSEVIER

International Journal of Solids and Structures 41 (2004) 351–363

INTERNATIONAL JOURNAL OF SOLIDS and STRUCTURES

www.elsevier.com/locate/ijsolstr

Incorrect initiation and propagation of failure in non-local and gradient-enhanced media

Angelo Simone [1], Harm Askes, Lambertus J. Sluys *

Faculty of Civil Engineering and Geosciences, Delft University of Technology, P.O. Box 5048, 2600 GA Delft, The Netherlands

Received 6 May 2003; received in revised form 10 September 2003

Abstract

Damage initiation and propagation in a class of non-local and gradient-enhanced media is investigated. In this contribution it is shown how the use of a non-local dissipation-driving state variable leads to an incorrect failure characterisation in terms of damage initiation and propagation. Damage initiation is analysed in detail for a class of non-local damage models—formulated in an integral and a differential format—by means of analytical considerations and numerical investigations in a mode-I problem. A numerical study on damage propagation is also presented for a shear band formation problem.

Keywords: Damage initiation; Damage propagation; Regularised media; Shear band

1. Introduction

Correct failure characterisation, in terms of damage initiation and propagation, is a fundamental property of any sound model. Considering failure initiation, a quantitative discrepancy between the response of a regularised and a standard continuum is accepted but a qualitative resemblance must be maintained. It is obvious that a wrong prediction of the correct location or moment of initiation may lead to a misrepresentation of the failure mode and therefore of the failure load. Failure propagation is as important as failure initiation and, in a continuous failure representation, gives an indication of the failure mechanism. A realistic failure propagation is of paramount importance when the assessment of a constitutive model is concerned.

When softening constitutive relationships are considered in a continuum mechanics framework some sort of regularisation technique must be employed to maintain well-posedness of the governing equations. A common technique relies on the introduction of non-local terms in the governing equations. In the class

* Corresponding author. Tel.: +31-15-278-2728; fax: +31-15-278-6383.
E-mail address: l.j.sluys@citg.tudelft.nl (L.J. Sluys).
[1] Supported through the BEO programme (special fund from Delft University of Technology for excellent research).

0020-7683/$ - see front matter © 2003 Elsevier Ltd. All rights reserved.
doi:10.1016/j.ijsolstr.2003.09.020

of non-local models analysed here (Engelen et al., 2003; Pamin et al., 2003; Peerlings et al., 1996; Pijaudier-Cabot and Bažant, 1987), only the dissipation-driving variable is given a non-local character.

Aim of this contribution is to show that the choice of a non-local quantity as damage-driving quantity produces non-physical damage initiation away from the crack tip in mode-I problems and a wrong failure pattern in shear band problems. Damage initiation in a class of non-local damage models, within an integral (Pijaudier-Cabot and Bažant, 1987) as well as a differential (Peerlings et al., 1996) formulation, is analysed. The findings of this study are not limited to damage mechanics but extend easily to other dissipation mechanisms, e.g. plasticity (Engelen et al., 2003; Pamin et al., 2003), if a similar form of regularisation is employed. This contribution is organised as follows: in Section 2 the damage models used for the derivations in Section 3 are recalled. In Sections 3.1 and 3.2 incorrect damage initiation in mode-I is proven analytically and illustrated numerically, respectively while incorrect damage propagation in shear band problems is illustrated numerically in Section 4.

2. Continuum damage theories

In isotropic damage models, material degradation is introduced through a reduction of the elastic stiffness via a scalar quantity ω ($0 \leqslant \omega \leqslant 1$) according to

$$\mathbf{D}^{\text{effective}} = (1-\omega)\mathbf{D}^{\text{el}}, \tag{1}$$

where $\mathbf{D}^{\text{el}}$ is the constitutive fourth order elasticity tensor. The isotropic damage parameter ω is a function of the monotonically increasing deformation history parameter κ, whose evolution is governed by the Kuhn–Tucker relations

$$\dot{\kappa} \geqslant 0, \quad e-\kappa \leqslant 0, \quad \dot{\kappa}(e-\kappa) = 0. \tag{2}$$

A local scalar measure e of the strain tensor can be defined (Mazars, 1984; Mazars and Pijaudier-Cabot, 1989) by

$$e = \sqrt{\sum_{i=1}^{3} \langle \varepsilon_i \rangle^2}, \tag{3}$$

with $\langle \varepsilon_i \rangle = (\varepsilon_i + |\varepsilon_i|)/2$ and ε_i the principal strains, or by the von Mises strain

$$e = \frac{1}{1+\nu}\sqrt{-3J_2}, \tag{4}$$

with ν the Poisson's ratio and the invariant J_2 of the strain tensor $\boldsymbol{\varepsilon}$ defined as

$$J_2 = \operatorname{tr}(\boldsymbol{\varepsilon}\cdot\boldsymbol{\varepsilon}) - \frac{1}{3}\operatorname{tr}^2(\boldsymbol{\varepsilon}). \tag{5}$$

In this study, damage evolution is governed by the exponential softening law (Peerlings et al., 1996)

$$\omega = 1 - \frac{\kappa_0}{\kappa}(1-\alpha+\alpha\exp(-\beta(\kappa-\kappa_0))) \quad \text{if } \kappa > \kappa_0, \tag{6}$$

with α and β model parameters and κ_0 the threshold of damage initiation.

In the non-local damage model proposed by Pijaudier-Cabot and Bažant (1987), damage initiation is driven by a non-local scalar measure $\tilde{e}$ of the strain tensor defined as

$$\tilde{e}(\mathbf{x}) = \frac{\int_\Omega \psi(\mathbf{y};\mathbf{x}) e(\mathbf{y})\,\mathrm{d}\Omega(\mathbf{y})}{\int_\Omega \psi(\mathbf{y};\mathbf{x})\,\mathrm{d}\Omega(\mathbf{y})}, \tag{7}$$

where ψ is a homogeneous and isotropic weight function for the non-local averaging. The normalised Gaussian function

$$\psi(\rho) = \frac{1}{2\pi l^2} \exp\left(-\frac{\rho^2}{2l^2}\right) \quad \text{in } \mathbb{R}^2, \tag{8}$$

where l sets how ψ decays away from $\rho = 0$ and ρ is defined as the distance between the points $\mathbf{y}$ and $\mathbf{x}$, is usually taken as the weight function in integral non-local models. Note that, with these definitions, the denominator in (7) sums to unity for an infinite and regular domain. In an approximated differential version of the non-local model implicit gradient-enhanced damage model by Peerlings et al. (1996), (7) is expanded in a Taylor's series around $\mathbf{x}$ which yields, after some manipulations and with the use of (8),

$$\tilde{e} - \frac{1}{2} l^2 \nabla^2 \tilde{e} = e \quad \text{in } \Omega. \tag{9}$$

Eq. (9) is complemented by the homogeneous natural boundary conditions

$$\nabla \tilde{e} \cdot \mathbf{n} = 0 \quad \text{on } \Gamma, \tag{10}$$

where $\mathbf{n}$ is the outward unit normal at the boundary Γ of Ω. The equivalence of (7) and (9) has been discussed by Peerlings et al. (2001). The non-local state variable $\tilde{e}$, defined either via (7) or via (9), replaces its local counterpart e in (2). Thus, non-locality is introduced in the model through the damage-driving state variable.

3. Damage characterisation in mode-I problems

Proper failure characterisation relies on correct failure initiation. In quasi-brittle failure analyses of notched specimens, experimental evidence shows that cracks propagate from the notch (van Mier, 1997). Proper modelling of quasi-brittle material behaviour must reproduce this phenomenon.

Damage initiation in mode-I is analysed by means of the compact tension specimen with a pre-existing crack of length h depicted in Fig. 1a. Numerical analyses showed that the elastic contour plots of the non-local damage-driving quantity $\tilde{e}$ is maximum at some distance from the crack tip. More specifically, the maximum of the non-local equivalent strain was found along the line $\overline{ab}$, as qualitatively depicted in Fig. 1b (analytical result) and in Fig. 2b (numerical result), and not at the crack tip. Thus, damage initiation is predicted inside the specimen, rather than at the crack tip. In Fig. 1b, the profiles of the local equivalent strain e and of the non-local equivalent strain $\tilde{e}$ (according to (7) and (9), respectively) are plotted along the line $\overline{ab}$. First, consider the profile of e. The local equivalent strain, as predicted by Griffith's theory, equals 0 from point a to the crack tip. At the crack tip it is infinite, after which it decays monotonically to its finite value at point b. The profile of the non-local counterpart $\tilde{e}$ differs from the profile of e in that (i) no singularity is present (as already noted by Peerlings et al. (2001)), and (ii) the maximum occurs not at the crack tip but at some point between the crack tip and point b along the crack line. Note that the crack is discretised as a set of zero measure in this example and, as such, along line $\overline{ab}$, it does not influence the integral in the denominator in (7)—the denominator in (7) is the normalising factor in the non-local averaging near free boundaries. In other words, for all points along line $\overline{ab}$ that are reasonably far from the edges of the specimen, the denominator of (7) yields the same value, therefore the shift of maximum from e to $\tilde{e}$ is not the result of a varying averaging volume. The shift of the maximum of the non-local equivalent strain $\tilde{e}$ from the crack tip is a phenomenon which is independent of the stress situation (plane stress/plane strain) and of the choice of the local equivalent strain definition as it will be illustrated in Section 3.2. Indeed, this can be explained by considering that non-local averaging of the unsymmetrical local strain field e is

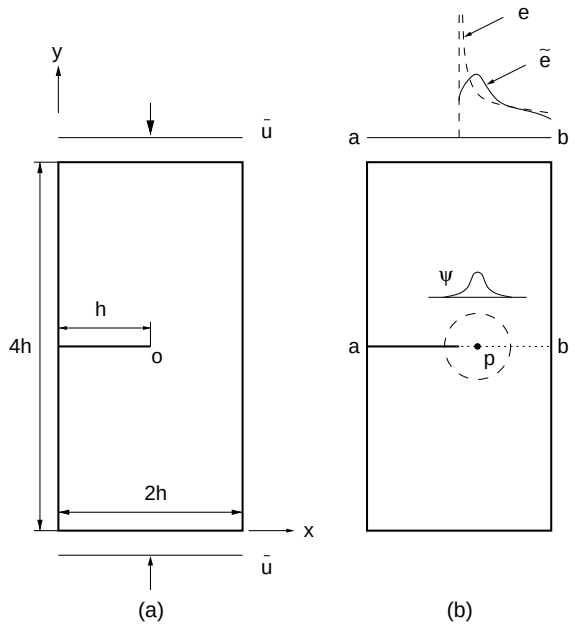

Fig. 1. Compact tension specimen: (a) geometry and boundary conditions and (b) local (e) and non-local ($\tilde{e}$) equivalent strain field along the crack line $\overline{ab}$.

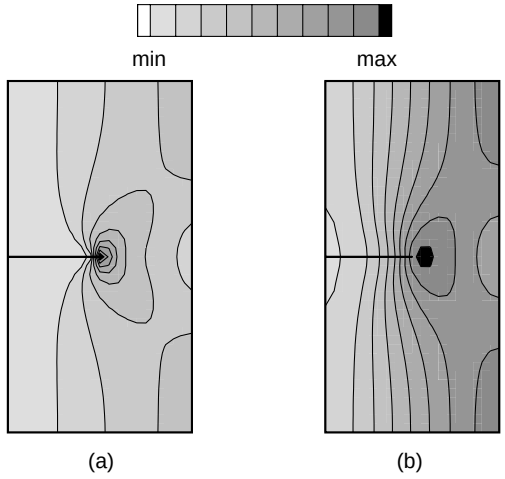

Fig. 2. Qualitative contour plot of (a) the local elastic equivalent strain e and (b) the non-local elastic equivalent strain $\tilde{e}$: due to the non-local averaging the maximum of the non-local equivalent strain shifts away from the tip.

performed through a symmetric function ψ. The shift of the maximum away from the crack tip will be proven analytically and illustrated numerically in Sections 3.1 and 3.2, respectively.

3.1. Analytical considerations

In the ideal situation of a planar crack in an infinite plate loaded in mode-I, such as the one depicted in Fig. 3, the linear elastic stress field is singular at the crack tip (Ewalds and Wanhill, 1984). Analytical manipulations under the assumption of a plane stress situation yield the Cartesian strains at a distance r and an angle θ from the crack tip o:

$$\varepsilon_{11}(r,\theta) = \frac{K_{\mathrm{I}}}{E\sqrt{2\pi r}} \cos\frac{1}{2}\theta\left(1 - \nu - (1+\nu)\sin\frac{1}{2}\theta\sin\frac{3}{2}\theta\right), \tag{11}$$

$$\varepsilon_{22}(r,\theta) = \frac{K_{\mathrm{I}}}{E\sqrt{2\pi r}} \cos\frac{1}{2}\theta\left(1 - \nu + (1+\nu)\sin\frac{1}{2}\theta\sin\frac{3}{2}\theta\right), \tag{12}$$

$$\varepsilon_{12}(r,\theta) = \frac{K_{\mathrm{I}}}{E\sqrt{2\pi r}} (1+\nu)\cos\frac{1}{2}\theta\sin\frac{1}{2}\theta\cos\frac{3}{2}\theta, \tag{13}$$

$$\varepsilon_{33}(r,\theta) = \frac{\nu}{\nu-1}(\varepsilon_{11}+\varepsilon_{22}) = -\frac{2\nu K_{\mathrm{I}}}{E\sqrt{2\pi r}}\cos\frac{1}{2}\theta, \tag{14}$$

from which the local equivalent strain (4) reads

$$e(r,\theta) = \frac{\sqrt{2}K_{\mathrm{I}}}{4E\sqrt{\pi r}}\sqrt{(1+\cos\theta)(5-3\cos\theta)}. \tag{15}$$

In the above relations, E is the Young's modulus, ν the Poisson's ratio and K_{I} the mode-I stress intensity factor.

Next, the non-local equivalent strain is investigated. First, its value at the crack tip is considered. Second, it will be shown that the crack tip value $\tilde{e}_0$ of $\tilde{e}$ is not maximum since larger values of $\tilde{e}$ occur at locations away from the crack tip. To demonstrate that damage initiation is incorrectly predicted with the class of non-local models analysed here, it is necessary and sufficient to demonstrate that the absolute maximum of the damage-driving quantity does not occur at the crack tip.

3.1.1. Crack tip value of non-local equivalent strain

Following Peerlings et al. (2001), it can be demonstrated that the non-local equivalent strain $\tilde{e}$ has a finite value $\tilde{e}_0$ at the crack tip. To this end, the two-dimensional normalised isotropic Gaussian weight function in (8) and the local equivalent strain expression in (15) are substituted in the non-local averaging of (7) to give

$$\tilde{e}_0 = \frac{K_{\mathrm{I}}}{8\pi^{3/2}El^2}\int_0^{\infty}\frac{1}{\sqrt{r}}\exp\left(-\frac{r^2}{2l^2}\right)r\,\mathrm{d}r\int_{-\pi}^{+\pi}\sqrt{2(1+\cos\theta)(5-3\cos\theta)}\,\mathrm{d}\theta. \tag{16}$$

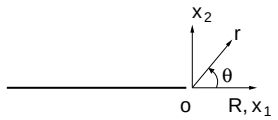

Fig. 3. Linear elastic crack problem in an infinite domain.

The first integral in (16) can be rewritten as

$$\int_0^{\infty} \sqrt{r} \exp\left(-\frac{r^2}{2l^2}\right) \mathrm{d}r = \frac{l^{3/2}\Gamma\left(\frac{3}{4}\right)}{\sqrt[4]{2}}, \tag{17}$$

where $\Gamma(\cdot)$ indicates the gamma function; the second integral in (16) yields:

$$\int_{-\pi}^{+\pi} \sqrt{2(1+\cos\theta)(5-3\cos\theta)}\,\mathrm{d}\theta = 8\sqrt{2} - \frac{2}{3}\sqrt{6}\ln(7-4\sqrt{3}). \tag{18}$$

Thus,

$$\tilde{e}_0 = \frac{K_\mathrm{I}}{E\sqrt{l}} \frac{\sqrt[4]{18}\Gamma\left(\frac{3}{4}\right)}{12\pi^{3/2}} [4\sqrt{3} - \ln(7-4\sqrt{3})] \approx 0.3612 \frac{K_\mathrm{I}}{E\sqrt{l}}, \tag{19}$$

which proves that the non-local equivalent strain is not singular at the crack tip (for $l \neq 0$). An analogous result was presented by Peerlings (1999, 2001). One of the conclusions reported by Peerlings (1999) is that the absolute maximum of the non-local equivalent strain is at the crack tip. This issue is discussed next.

3.1.2. Non-local equivalent strain determination away from the crack tip

The search for larger values of the non-local equivalent strain is restricted to the points along the crack line $\overline{ab}$ (see Fig. 2b). A point p is considered along line $\overline{ab}$ whereby the distance from the crack tip to p is denoted by R. The weight function in (8) is written for a point p as

$$\psi_p(r,\theta,R) = \frac{1}{2\pi l^2} \exp\left(-\frac{(r\cos\theta - R)^2 + (r\sin\theta)^2}{2l^2}\right), \tag{20}$$

and with this expression the non-local equivalent strain at a distance R from the crack tip along the crack line reads

$$\tilde{e}_R = \int_0^{\infty}\int_{-\pi}^{+\pi} \psi_p(r,\theta,R) e(r,\theta) r\,\mathrm{d}\theta\,\mathrm{d}r, \tag{21}$$

for which a closed form solution could not be obtained. Numerical evaluation of the integral in (21), for a given R, indicates that the maximum of the non-local equivalent strain is not positioned at the crack tip (see Fig. 4a). The linear dependence of the position of the maximum of the non-local equivalent strain upon the length scale l is depicted in Fig. 4b which shows that the non-local equivalent strain is maximum at the crack tip only for $l = 0$ mm, i.e. only for a local damage model. These results extend to a finite specimen width if the effect of a finite geometry is reflected in the stress intensity factor K_I.

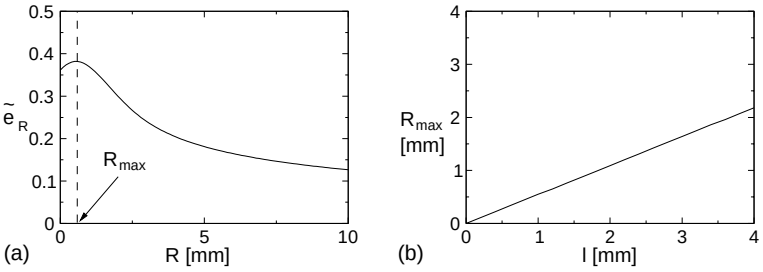

Fig. 4. Non-local equivalent strain at distance R from the tip for $l = 1$ mm (a) and linear dependence of the position of the maximum of the non-local equivalent strain $R_{\max}$ upon the length scale l (b) for unit values of E and K_I.

Note that, in general, the use of non-local averaging of field quantities with isotropic weight functions results in a modification of failure characterisation. In the class of non-local elasticity models proposed by Eringen et al. (1977), the stress field value at the crack tip is finite but, similar to the non-local damage model considered here, its maximum occurs at some distance from the crack tip along the crack line. The modification of the weight function ψ in order to preserve the qualitative character of the field to be averaged (the local field) is problematic and leads to tailor-made solutions which are not recommended when a differential version of the non-local damage model is considered.

3.2. Numerical analysis

The compact tension specimen depicted in Fig. 1a has been numerically analysed by using an integral and a differential non-local damage model with the finite-element method. In the numerical simulations only the upper part of the specimen has been discretised due to symmetry, and the load has been applied via an imposed displacement. The following material parameters have been adopted for the simulation: Young's modulus $E = 1000$ MPa; Poisson's ratio $\nu = 0$; exponential damage evolution law (6) with threshold of damage initiation $\kappa_0 = 0.0003$; softening parameters $\alpha = 0.99$ and $\beta = 1000$; length scale $l = 0.2$ mm. The equivalent strain definition according to (3) has been used. The height of the specimen has been taken as $4h = 2$ mm. The mesh used for the simulations has been chosen such that a sufficient resolution of the non-local field is obtained. More details on the finite-element implementation of the differential non-local model can be found in Peerlings et al. (1996).

Contour plots of the non-local equivalent strain at the onset of damage initiation are reported in Fig. 5. Clearly, the maximum of the non-local equivalent strain has shifted, both for the integral model and the differential model. Due to the shifting, damage is expected to initiate, wrongly, away from the crack tip. However, as depicted in Fig. 6, damage profiles close to global failure of the specimen give no indication of the incorrect damage initiation. Experience with the differential version of the non-local damage model indicates that this is a common situation in mode-I problems and that failure characterisation close to failure is quite similar to the ones obtained with other constitutive models. Consequently, the shift of the maximum of the non-local equivalent strain away from the crack tip can be considered 'harmless' as long as the final failure characterisation is concerned. However, it must be realised that the use of a non-local dissipation-driving variable leads to a non-physical damage initiation. The shift of the maximum of the non-local equivalent strain away from the crack tip is present, although less evident, also in case of cracks

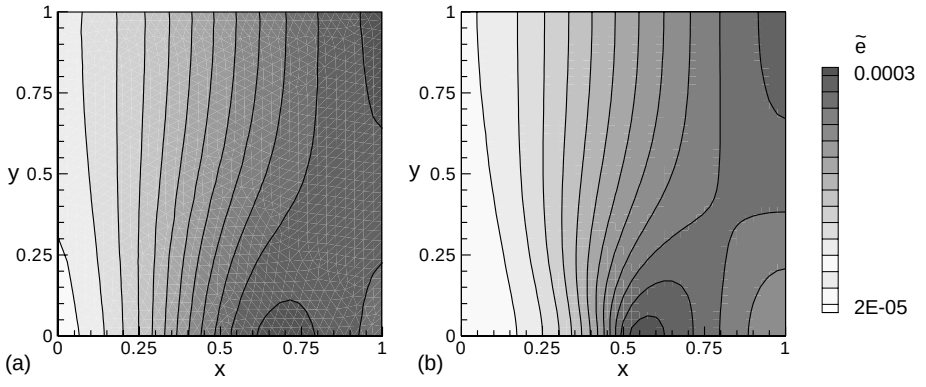

Fig. 5. Contour plot of the non-local equivalent strain for the (a) integral non-local damage and the (b) differential non-local damage model at the onset of damage initiation, i.e. in the elastic stage (measures in mm; crack tip at $x = 0.5$ mm).

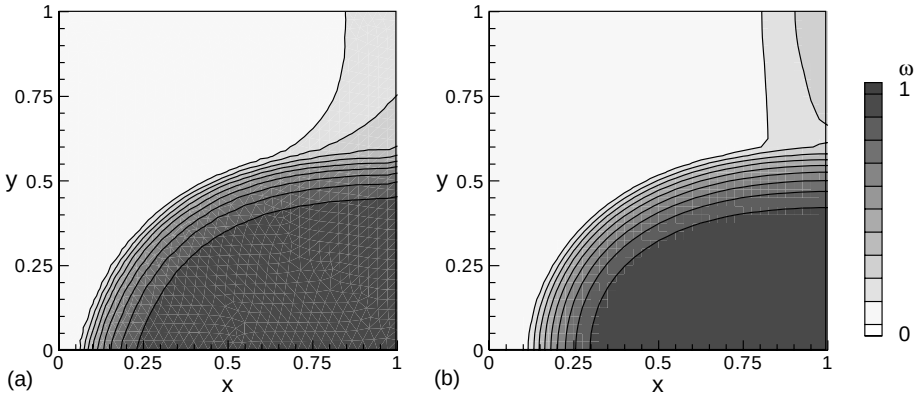

Fig. 6. Contour plot of the damage field for the (a) integral non-local damage and the (b) differential non-local damage model close to failure (measures in mm; crack tip at $x = 0.5$ mm).

or notches modelled as strongly non-convex entities with non-zero volume, i.e. when there are no strain singularities.

4. Damage characterisation in shear band problems

The correct determination of shear bands is of prime interest and it is directly linked to the occurrence of possible collapse mechanisms in many engineering problems. Specimen under compressive loading are usually characterised by the formation of shear bands whose inclination can be determined analytically. Results obtained within the flow theory of plasticity (Runesson et al., 1991) have been extended to scalar damage models by Rizzi et al. (1995) and Carol and Willam (1997) and apply to an infinite geometry for a standard (i.e. not regularised) medium. Their results have been derived for a specific choice of the equivalent strain definition and their generalisation to other equivalent strain definitions, although possible in principle, is not within the scope of this study and therefore is not considered here. In what follows, it is illustrated how non-local regularisation techniques significantly alter failure propagation during strain localisation.

To illustrate the problem, shear band simulations under a plane stress and a plane strain configuration have been performed with the gradient-enhanced continuum damage model described in Section 2 for the two-dimensional specimen depicted in Fig. 7. Both geometries were considered to assess the validity of the boundary condition (10) which was indeed verified: both geometries gave identical results and in the following only the geometry in Fig. 7b is considered. A detailed analysis regarding the treatment of the non-local equivalent strain at the boundaries for a mode-I problem was given by Peerlings et al. (2001).

In numerical simulations of quasi-static shear band formation under compressive loading, shear bands are usually triggered by an imperfection (placed on the left bottom corner for the specimen in Fig. 7b). After the shear band has been initiated, expansion of the plastic zone and further localisation within the plastic zone is observed (Zervos et al., 2001) (for a schematic initiation and evolution of the shear band, see Fig. 8). This characterisation is valid in the context of a continuous failure description. When a discrete approach to failure is considered (Borja, 2000), the characterisation is quite similar with the difference that there is no 'measure' of the shear band in the direction perpendicular to the propagation direction (in other words, the shear band is there considered as a discontinuity and, as such, it is collapsed into a line). Shear bands are characterised by their stationary nature in the sense that their position is determined after their formation (see Nemat-Nasser and Okada (2001) and references herein for experimental shear bands and

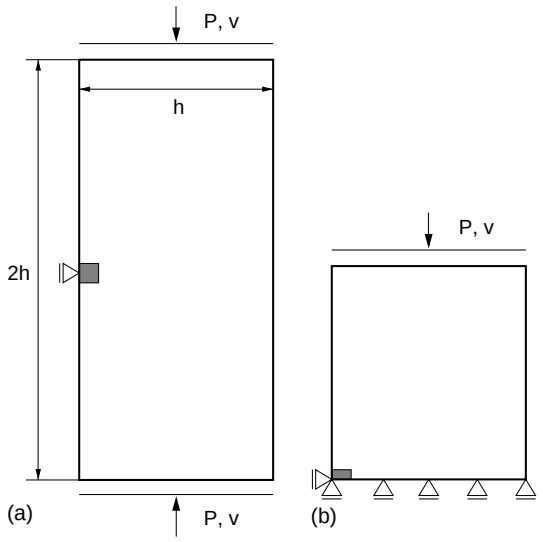

Fig. 7. Geometry and boundary conditions for the specimen in biaxial compression: (a) full specimen and (b) half specimen. The shaded part indicates the imperfection ($h = 60$ mm; imperfection size in (a) is $h/10 \times h/10$).

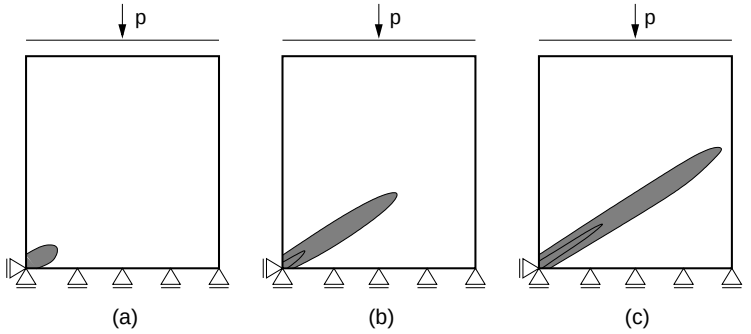

Fig. 8. Schematic formation of a shear band: (a) initiation and (b) expansion of the plastic zone and (c) further localisation/expansion within/of the plastic zone (strain localisation is triggered by a weak spot in the left bottom corner).

Borja (2000), Garaizar and Trangenstein (1998), Needleman and Tvergaard (1984), Ortiz et al. (1987), Sluys (1992), Tvergaard et al. (1981), Wells and Sluys (2002), Zervos et al. (2001) for some numerical results). The inclination angle that the shear band forms with the horizontal axis is determined mainly by assumptions related to the constitutive model, to the Poisson's ratio and to the plane stress or plane strain condition (Carol and Willam, 1997; Rizzi et al., 1995; Runesson et al., 1991; Sluys, 1992) while the width of the shear band, in a continuous description of failure, is dictated by the length scale (i.e. the larger the length scale, the wider the band width).

In the numerical analyses, the material has been characterised by a Young's modulus $E = 20{,}000$ MPa, a Poisson's ration $v = 0.2$, the exponential softening law (6) with $\kappa_0 = 0.0001$, $\alpha = 0.99$ and $\beta = 300$ and the von Mises equivalent strain (4). The load has been applied via displacement control. The imperfection has been given a reduced value of κ_0 ($\kappa_0 = 0.00005$) and the mesh density has been chosen to ensure a sufficient resolution of the non-local field. To begin with, the evolution of the shear band, in terms of non-local equivalent strain and damage fields has been analysed for the specimen in Fig. 7b with a length scale

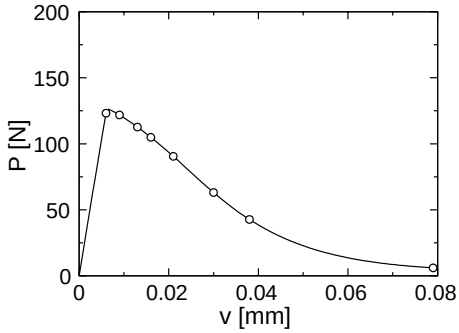

Fig. 9. Load–displacement curve for the shear band problem (relevant fields corresponding to the white circles are depicted in Figs. 10 and 11).

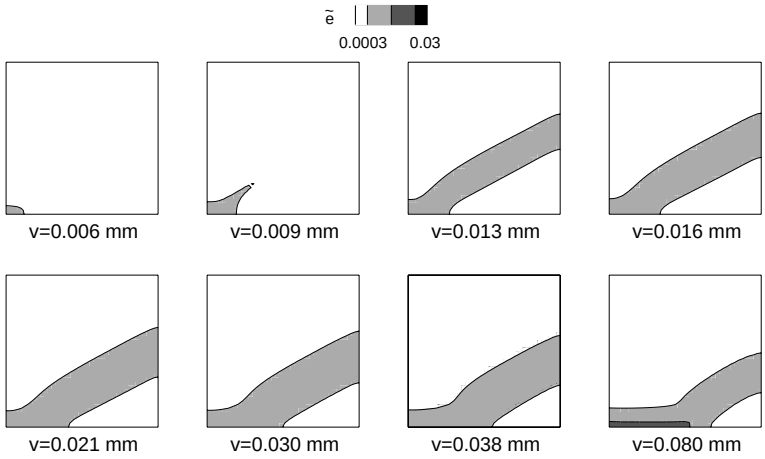

Fig. 10. Shear band evolution: contour plots of the non-local equivalent strain field (see Fig. 9).

$l = 2$ mm under a plane strain condition. Results depicted in Figs. 10 and 11 relate to the load–displacement diagram in Fig. 9, where the applied load P is plotted against the absolute value v of the vertical displacement. In the contour plots in Figs. 10 and 11, only values larger than the threshold in the respective legends have been plotted. It is clear how the shear band 'migrates' from the weak spot, where it was initiated, to the opposite side of the specimen along the horizontal boundary as depicted in Figs. 10 and 11. Similar results have been reported in Engelen et al. (2003) and Pamin et al. (2003). It is stressed that the 'migrating' shear band is not the product of an improper treatment of the boundary conditions since, as already stated before, the geometries reported in Fig. 7 give identical results. This particular appearance of the shear band is simply due to a wrong prediction of the positioning of localised shearing and has the same nature of the shift of the maximum of the non-local equivalent strain in mode-I problems.

The effect of a larger length scale is reported in Fig. 12 together with a comparison between plane stress and plane strain conditions close to failure. Similar to shear bands in a plasticity context (Runesson et al., 1991) and as reported by Carol and Willam (1997), the only noticeable difference between plane stress and plane strain resides in a different inclination of the shear band with respect to the horizontal axis which does not correspond to the numerical results in Fig. 12. Further, with an increasing non-local effect a wider shear band width is expected, while it is also noted that a more pronounced shift of the shear band takes place. In

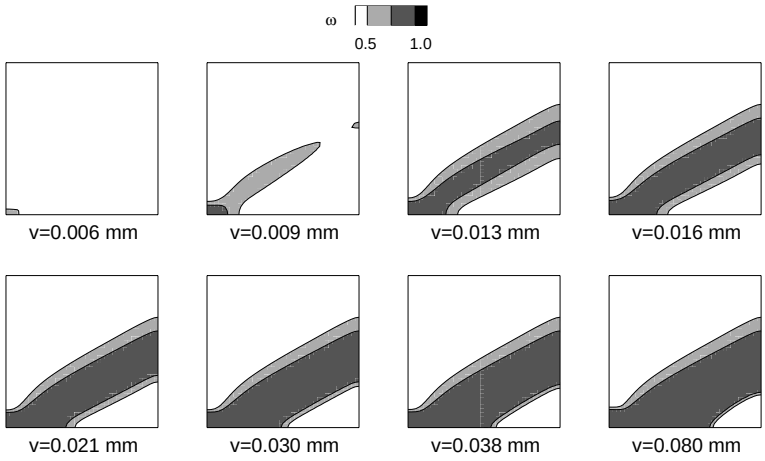

Fig. 11. Shear band evolution: contour plots of the damage field (see Fig. 9).

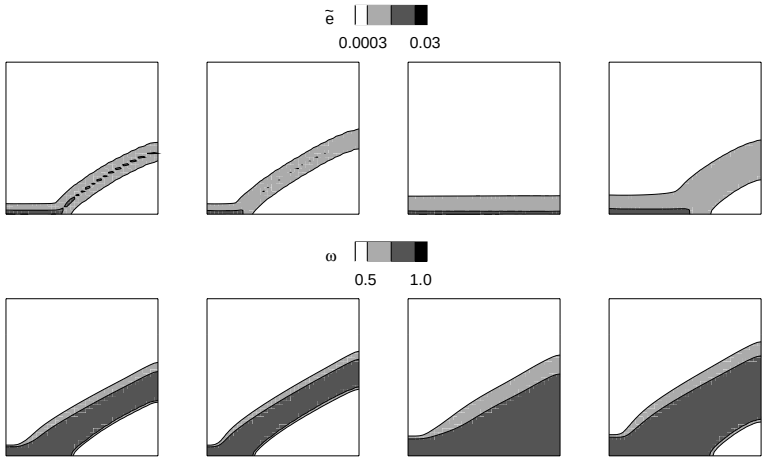

Fig. 12. Shear band close to failure: contour plots of the non-local equivalent strain field (top) and of the damage field (bottom) for $l = 1$ mm (left) and $l = 2$ mm (right) for plane stress (odd columns) and plane strain (even columns).

one case (plane stress situation with $l = 2$ mm) the non-local equivalent strain field mimics a mode-I situation and almost half of the specimen is damaged, which is not realistic.

5. Concluding remarks

The analysis of failure characterisation in a class of non-local damage models has been the subject of this contribution. It has been shown that the use of a non-local variable as dissipation-driving variable predicts incorrect failure initiation and propagation. This issue has been investigated through analytical and numerical analyses for mode-I and shear band problems. The particular choice of the examples in mode-I failure was aimed at emphasising that the standard formulation of non-local damage model, either in

integral (Pijaudier-Cabot and Bažant, 1987) or in differential (Peerlings et al., 1996) format, is unsuited to correctly describe damage initiation when degradation stems from a strong inhomogeneity of the strain field. It is stressed that this phenomenon is not caused, in the present case, by boundary effects on the non-local averaging. Analogous results can be found in cases with strong gradients of the quantity to be averaged due to e.g. concave boundaries, concentrated loads and material inhomogeneities. Although the shift of the maximum of the dissipation-driving variable may not alter the final failure representation in mode-I dominated problems, it does affect the transition from continuous to continuous-discontinuous failure in a gradient-enhanced damage model as discussed by Simone et al. (2003a,b). The numerical study of a shear band problem illustrated that the non-local averaging is responsible for the non-stationary shear band which results in an unrealistic failure pattern. This has been studied for various length scale values under plane stress and plane strain conditions.

To summarise, constitutive models based on a non-local dissipation-driving variable may lead to unrealistic failure representations due to a fundamental flaw in the damage initiation and evolution.

Acknowledgements

Stimulating discussions with A.V. Metrikine (Delft University of Technology) and R.H.J. Peerlings (Eindhoven University of Technology) are gratefully acknowledged.

References

Borja, R.I., 2000. A finite element model for strain localization analysis of strongly discontinuous fields based on standard Galerkin approximation. Computer Methods in Applied Mechanics and Engineering 190, 1529–1549.

Carol, I., Willam, K., 1997. Application of analytical solutions in elasto-plasticity to localization analysis of damage models. In: Owen, D.R.J., Oñate, E., Hinton, E. (Eds.), Computational Plasticity, Fundamentals and Applications. CIMNE, Barcelona, Spain, pp. 714–719.

Engelen, R.A.B., Geers, M.G.D., Baaijens, F.P.T., 2003. Nonlocal implicit gradient-enhanced elasto-plasticity for the modelling of softening behaviour. International Journal of Plasticity 19 (4), 403–433.

Eringen, A.C., Speziale, C.G., Kim, B.S., 1977. Crack-tip problem in non-local elasticity. Journal of the Mechanics and Physics of Solids 25, 255–339.

Ewalds, H.L., Wanhill, R.J.H., 1984. Fracture Mechanics. Edward Arnold, London, England.

Garaizar, F.X., Trangenstein, J., 1998. Adaptive mesh refinement and front-tracking for shear bands in an antiplane shear model. SIAM Journal on Scientific Computing 20 (2), 750–779.

Mazars, J., 1984. Application de la Mécanique de l'Endommagement au Comportement Non-Linéaire et à la Rupture du Béton de Structure, PhD Thesis, Université Paris VI, France.

Mazars, J., Pijaudier-Cabot, G., 1989. Continuum damage theory—application to concrete. Journal of Engineering Mechanics 115, 345–365.

Needleman, A., Tvergaard, V., 1984. Finite element analysis of localization in plasticity. In: Oden, J.T., Carey, G.F. (Eds.), Finite Elements: Special Problems in Solid Mechanics, vol. V. Prentice-Hall Inc., Englewood Cliffs, NJ, pp. 94–157.

Nemat-Nasser, S., Okada, N., 2001. Radiographic and microscopic observation of shear bands in granular materials. Géotechnique 51 (9), 753–765.

Ortiz, M., Leroy, Y., Needleman, A., 1987. A finite element method for localized failure analysis. Computer Methods in Applied Mechanics and Engineering 61, 189–214.

Pamin, J., Askes, H., de Borst, R., 2003. Two gradient plasticity theories discretized with the element-free Galerkin method. Computer Methods in Applied Mechanics and Engineering 192, 2377–2403.

Peerlings, R.H.J., 1999. Enhanced Damage Modelling for Fracture and Fatigue, PhD thesis, Eindhoven University of Technology.

Peerlings, R.H.J., de Borst, R., Brekelmans, W.A.M., de Vree, J.H.P., 1996. Gradient-enhanced damage for quasi-brittle materials. International Journal for Numerical Methods in Engineering 39, 3391–3403.

Peerlings, R.H.J., Geers, M.G.D., de Borst, R., Brekelmans, W.A.M., 2001. A critical comparison of nonlocal and gradient-enhanced softening continua. International Journal of Solids and Structures 38, 7723–7746.

Pijaudier-Cabot, G., Bažant, Z.P., 1987. Nonlocal damage theory. Journal of Engineering Mechanics 113, 1512–1533.

Rizzi, E., Carol, I., Willam, K., 1995. Localization analysis of elastic degradation with application to scalar damage. Journal of Engineering Mechanics 121 (4), 541–554.

Runesson, K., Ottosen, N.S., Peric, D., 1991. Discontinuous bifurcation of elasto-plastic solutions in plane stress and plane strain. International Journal of Plasticity 7, 99–121.

Simone, A., Wells, G.N., Sluys, L.J., 2003a. Discontinuities in regularised media. In: Owen, D.R.J., Oñate, E., Suárez, B. (Eds.), Proceedings of the Seventh International Conference on Computational Plasticity—Complas 2003, CIMNE, Barcelona, Spain, 7–10 April, On CD-ROM, p. 90.

Simone, A., Wells, G.N., Sluys, L.J., 2003b. From continuous to discontinuous failure in a gradient-enhanced continuum damage model. Computer Methods in Applied Mechanics and Engineering 192 (41–42), 4581–4607.

Sluys, L.J., 1992. Wave Propagation, Localisation and Dispersion in Softening Solids, PhD Thesis, Delft University of Technology.

Tvergaard, V., Needleman, A., Lo, K.K., 1981. Flow localization in the plane strain tensile test. Journal of the Mechanics and Physics of Solids 29 (2), 115–142.

van Mier, J.G.M., 1997. Fracture Processes of Concrete. CRC Press, Inc, Boca Raton, Florida.

Wells, G.N., Sluys, L.J., de Borst, R., 2002. Simulating the propagation of displacement discontinuities in a regularised strain-softening medium. International Journal for Numerical Methods in Engineering 53 (5), 1235–1256.

Zervos, A., Papanastasiou, P., Vardoulakis, I., 2001. A finite element displacement formulation for gradient elastoplasticity. International Journal for Numerical Methods in Engineering 50, 1369–1388.